Nano Research
2020, 13(10): 2691–2696
ISSN 1998-0124 CN 11-5974/O4
https://doi.org/10.1007/s12274-020-2911-9

Research Article

Trimetallic Au@PdPb nanowires for oxygen reduction reaction

Xian Jiang[1,2,3], Yuexin Xiong[3], Ruopeng Zhao[2], Jiancheng Zhou[1] (✉), Jong-Min Lee[2] (✉), and Yawen Tang[3] (✉)

[1] School of Chemistry and Chemical Engineering, Southeast University, Nanjing 211189, China
[2] School of Chemical and Biomedical Engineering, Nanyang Technological University, Singapore 637459, Singapore
[3] Jiangsu Key Laboratory of New Power Batteries, Jiangsu Collaborative Innovation Center of Biomedical Functional Materials, School of Chemistry and Materials Science, Nanjing Normal University, Nanjing 210023, China

Received: 21 April 2020 / **Revised:** 26 May 2020 / **Accepted:** 30 May 2020

ABSTRACT

The development of highly efficient and stable Pd-based catalysts is crucial to improve their sluggish oxygen reduction reaction (ORR) kinetics in acid media. To improve ORR activity and utilization efficiency of Pd, an ideal catalyst should have ORR-favorable chemical environment, optimized geometric structure, and long periods of operation. In this work, we first synthesize a novel trimetallic Au@PdPb core–shell catalyst consisting of PdPb alloy nano-layers grown on the surface of ultrathin Au nanowires (NWs) by a two-step water-bath method. The Au@PdPb NWs have the merits of anisotropic one-dimensional nanostructure, high utilization efficiency of Pd atoms and doping of Pb atoms. Because of the structural and multiple compositional advantages, Au@PdPb NWs exhibit remarkably enhanced ORR activity with a high half-wave potential (0.827 V), much better than those of commercial Pd black (0.788 V) and bimetallic Au@Pd NWs (0.803 V). Moreover, Au@PdPb NWs display better electrocatalytic stability for the ORR than those of Pd black and Au@Pd NWs. This study demonstrates the validity of our approach for deriving highly ORR-active Pd-based catalysts by modifying their structure and composition.

KEYWORDS

trimetallic Au@PdPb nanowires, core–shell structure, optimized electronic structure, electrocatalyst, oxygen reduction reaction

1 Introduction

Boosting oxygen reduction reaction (ORR) kinetics in acid electrolyte has crucial significance for overcoming the bottlenecks in cathodic development of the proton exchange membrane fuel cells (PEMFCs) [1–3]. Pd has been widely reported for the appreciable ORR performance in alkline media [4, 5]. However, the ORR activity and stability of Pd in acidic media are not satisfactory due to the intrinsic electronic structure and improper d-band center [6, 7]. Rational design of Pd-based core–shell structure based on manuipulation of Pd electronic structure can endow Pd with significantly improved activity and stability [8–11]. Recently, core–shell Au@Pd catalysts have been broadly investigated to assume significantly promoted electrochemical activity and durablity via altering the electronic structure of Pd [12–17]. For instance, Yang et al. reported Au@Pd nanoparticles with only three Pd atomic layers, which display superior ORR activity and stability induced by the lattice tensile effect between the PdAu interfaces than commercial Pd/C [18]. More recently, Xing et al. reported that sea urchin-like Au@Pd exihits 8.8 times higher current density towards formic acid oxidation than commercial Pd black and superior stability, which are abscribed to the suitable lattice strain between Pd and Au and more exposed active sites [17]. The introductionof Pb is useful to improve the utilization and activity of noble metal Pd [12, 19]. Huang et al. presented that coupled s-p-d exchange on Pd_3Pb tripods dominated by {111} planes boosts the ORR electrocatalysis in alkine media [6]. For futher improvement of electrocatalytic performance, numberous trimetallic electrocatalysts based on AuPd have been reported, which have better ORR activity than bimetallic counterparts because of their synergistic effects of the multiple components, such as Au@PdPt [20], Au@PdAg [21], AuPdNi [22], and AuPdCo [23], etc. Incorporating Au into bimetallic nanostructures (such as Au@PdPt) can enhance the ORR electrocatalytic performance and the stability of catalysts in acid electrolyte [24].

On the other hand, both ORR activity and stability can be improved by tailoring the geometrical factors through the creation of specific nanostructures [25–28]. It is well known that one-dimensional (1D) anisotropic nanowires can favor the mass/electron transfer and increase the atomic utilization [29–32]. Generally, nanowires possess tremendous defects, such as atom steps, grain boundaries, and high index facets, which can work as active sites owing to more exposed atoms on the edges for facilitating electrocatalytic activity [33, 34]. In addition, anisotropic 1D structure is more effective at preventing dissolution, aggregation, and Ostwald ripening than zero-dimensional (0D) nanoparticles for long-term operation [35, 36], and is convenient for enhancement of stability of catalysts. Based on the above disscusion, the integration of anisotropic 1D nanostructure and multiple component into Pd-based catalysts may provide a potential solution for improving ORR performance in acid media. However, current studies on the synthesis of 1D multi-component Pd-based core–shell nanostructures are insufficient, thus the exploration of facile and effective synthetic approaches is vital for future electro-catalyst design.

Address correspondence to Jiancheng Zhou, jczhou@seu.edu.cn; Jong-Min Lee, jmlee@ntu.edu.sg; Yawen Tang, tangyawen@njnu.edu.cn

Herein, we designed and developed core–shell trimetallic Au@PdPb catalyst with anisotropic 1D nanostructure (Au@PdPb nanowires (NWs)) by a two-step water-bath method under 60 °C. During the synthesis, ultrathin Au NWs were pre-fabricated as the template, and then PdPb alloy layers were reduced gradually on the surface of Au NWs in the assistance of L-ascorbic acid (AA). To our best knowledge, 1D trimetallic Au@PdPb nanostructures have rarely been reported to date. This method can be also used to fabricate bimetallic Au@Pd NWs. By virtue of the anisotropic 1D structure and synergistic effect of multi-components, the Au@PdPb NWs exhibit superior ORR activity and stability than those of commercial Pd black and bimetallic Au@Pd NWs.

2 Results and discussion

Figure 1(a) illustrates the fabrication of ultrathin core–shell Au@PdPb NWs. One-component Au NWs were firstly acquired by aging a mixed solution of $HAuCl_4$ aqueous solution and 1-naphthol ethanol solution. The rapid coordination-induced formation of Au nanowire-arrayed microspheres and their gradual dissociation during washing are responsible for the formation of ultrathin Au NWs [30]. By adding the $PdCl_2$ and $Pb(NO_3)_2$ aqueous solution into the as-prepared Au NWs solution with the reduction of AA, the Au@PdPb NWs were successfully fabricated (details are in the experimental section in the electronic supplementary material (ESM)). For comparison, bimetallic Au@Pd NWs were also prepared using a similar synthetic method. Figure 1(b) shows the X-ray diffraction (XRD) patterns of Au, Au@Pd, and Au@PdPb NWs, respectively. XRD pattern of Au NWs displays four typical peaks attributable to a face-centered cubic (fcc) phased Au (JCPDS no. 65-2870), while XRD pattern of Au@Pd and Au@PdPb NWs have some additional weak shoulder peaks (arrow mark in Fig. 1(b) and dotted box mark in Fig. S1 in the ESM), respectively, which may be caused by the formation of Pd and PdPb layer. The XRD results indicate the possible formation of core–shell Au@Pd and Au@PdPb structure.

Electronic microscope techniques were firstly conducted to characterize the ultrathin Au NWs. Large-scale scanning electron microscopy (SEM) verifies the uniform 1D morphology of the Au NWs (Fig. 2(a)), in accordance with the results of transmission electron microscopy (TEM) and scanning TEM (STEM) images (Figs. S2(a) and S2(b) in the ESM). Almost no other morphologies but ultrathin 1D nanowires can be observed, demonstrating the high yield of Au NWs. The average diameter of Au NWs was calculated to be about 4.8 nm according to Fig. 2(b) and Figs. S2(c) and S2(d) in the ESM. The metastable property of Au and uniform 1D ultrathin nanostructure make Au NWs a good template to induce the epitaxial growth of PdPb alloy shells. After the epitaxial growth of PdPb layers on the Au NWs surface, Au@PdPb NWs retain the structure and morphology integrity of 1D nanowires (Fig. 2(c)). Owing to the wrap of PdPb alloy layer, the surface of Au@PdPb NWs is rough

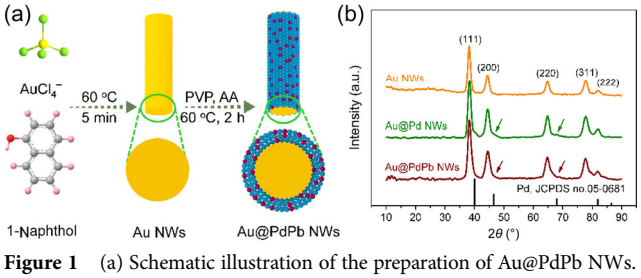

Figure 1 (a) Schematic illustration of the preparation of Au@PdPb NWs. (b) XRD patterns of Au, Au@Pd, and Au@PdPb NWs.

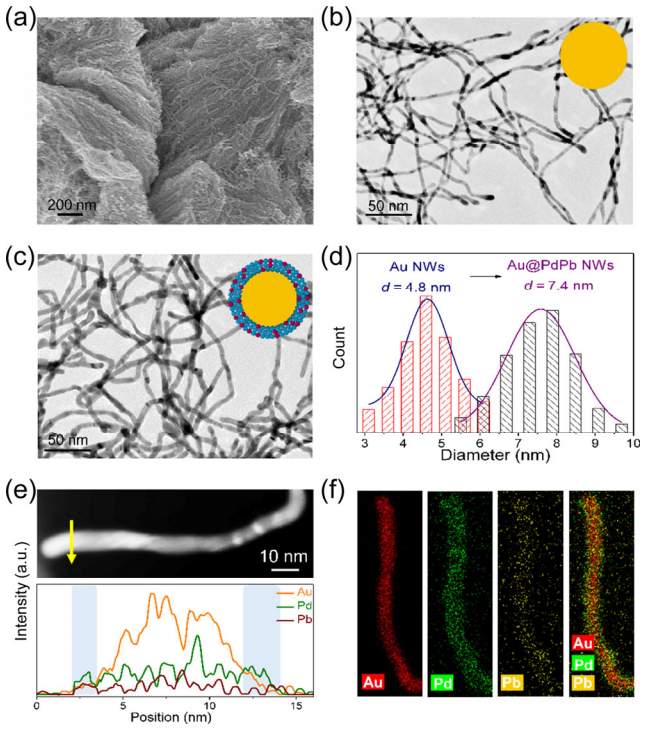

Figure 2 (a) SEM and (b) TEM image of ultrathin Au NWs. (c) TEM image of Au@PdPb NWs. (d) Histogram of particle-size distribution change from Au NWs to Au@PdPb NWs. (e) STEM image and EDX line-scan profile. (f) EDX elemental mapping images of a single Au@PdPb NW.

compared with that of Au NWs (Figs. S3(a) and S3(b) in the ESM). Figure 2(d) shows the histogram of particle-size distribution change from Au NWs to Au@PdPb NWs. The average diameter of Au@PdPb NWs (7.4 nm) was increased by about 2.6 nm compared with that of Au NWs (4.8 nm), which indicates the average thickness of PdPb layer of about 2.6 nm. To clearly demonstrate the formation of the core–shell structure, energy dispersive X-ray (EDX) line-scan profile and elemental mappings were performed. The thin PdPb alloy layer of about 3 nm was clearly observed to be covered on the Au NW surface (Fig. 2(e)). The signals of Pd and Pb surround around the Au NW in the EDX element mapping images (Fig. 2(f)), confirming the successful formation of the Au@PdPb core–shell structure. EDX spectrum (Fig. S4 in the ESM) indicates the atomic content of Au, Pd, and Pb in Au@PdPb NWs to be 62.4:25.6:12.0, which is very close to the feeding ratio of the metal precursors except for the less amount of Pb. Benefited from the unique 1D core–shell structure and trimetallic composition, the fabricated Au@PdPb NWs are expected to be an efficient catalyst for the electrocatalysis.

The synthetic method was also used to fabricate bimetallic Au@Pd NWs. The uniform 1D wire-like structure was clearly observed in a TEM image (Fig. 3(a)). Magnified TEM image depicts rough shell surface with a wide distribution thickness on the surface of Au NWs (core–shell boundary is marked with orange lines in Fig. S5 in the ESM). The particle-size variation from Au NWs to Au@Pd NWs was clearly demonstrated in Fig. 3(b) turning from 4.8 into 7.7 nm, implying the average thickness of Pd layers is about 3 nm. EDX line-scan profile (Fig. 3(c)) and element mapping images (Fig. 3(d)) of a single Au@Pd NW were also conducted to confirm the Au@Pd core–shell structure, in which Pd element was uniformly distributed around the Au NW. Furthermore, the element composition of Au and Pd in Au@Pd NWs were determined by the EDX

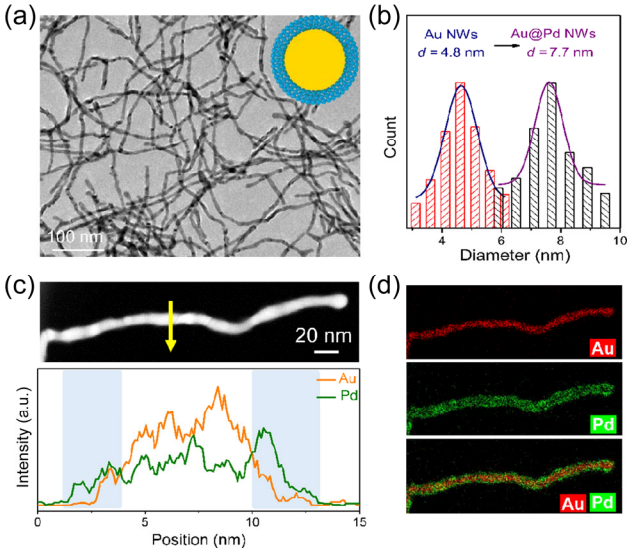

Figure 3 Physical characterization of Au@Pd NWs: (a) TEM image of Au@Pd NWs, (b) histogram of particle-size distribution change from Au NWs to Au@Pd NWs, (c) STEM image and EDX line-scan profile, and (d) EDX elemental mapping images of a single Au@Pd NW.

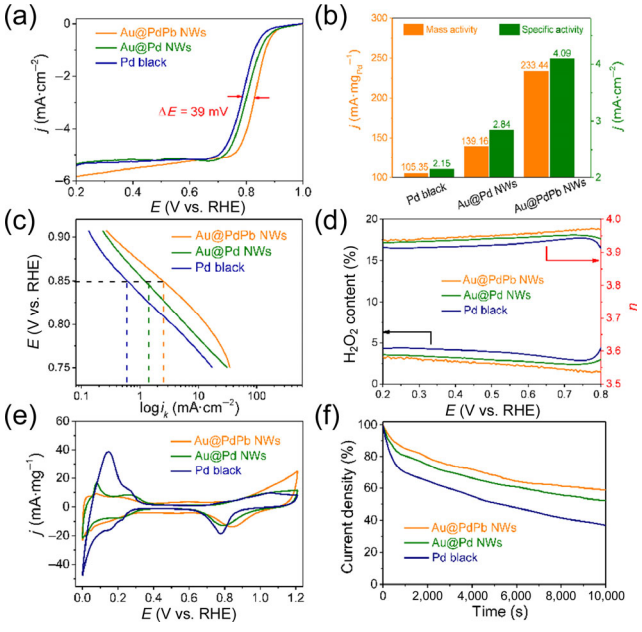

Figure 4 Comparation of the ORR performance of Au@PdPb NWs, Au@Pd NWs and Pd black in O_2-saturated 1.0 M $HClO_4$ solution: (a) ORR curves, (b) histograms of mass and specific activity of ORR under 0.85V, (c) Tafel plots, (d) electron transfer number n and HO_2^- yield in ORR, (e) CV curves, and (f) chronoamperometric measurements recorded under 0.5 V.

spectrum (Fig. S6 in the ESM) to be 60.1% and 39.9%, respectively, in good agreement with the Au/Pd feeding ratio.

To investigate ORR performance of trimetallic Au@PdPb NWs, liner sweep voltammetry (LSV) curves were performed by using rotating disk electrode (RDE) in an O_2-saturated 1.0 M $HClO_4$ solution. Bimetallic Au@Pd NWs and commercial Pd black were also included for comparison. As depicted in Fig. 4(a), both Au@PdPb NWs and Au@Pd NWs have more positive shifts than commercial Pd black. The half-wave potential ($E_{1/2}$) of Au@PdPb NWs is about 0.827 V, which is larger than those of Au@Pd NWs ($E_{1/2}$ = 0.803 V) and commercial Pd black ($E_{1/2}$ = 0.788 V). In addition, we calculated the mass and specific activity of Au@PdPb NWs, Au@Pd NWs, and commercial Pd black for further comparation, as listed in the histogram in Fig. 4(b). The mass activity for Au@PdPb NWs (233.44 mA·mg^{-1}) at 0.85 V is 1.68 and 2.22 times higher than those of Au@Pd NWs (139.16 mA·mg^{-1}) and commercial Pd black (105.35 mA·mg^{-1}), respectively (Fig. 4(b)). The specific activity of the Au@PdPb NWs can reach 4.09 mA·cm^{-2} at 0.85 V, 1.44 and 1.90 times higher than those of Au@Pd NWs (2.84 mA·cm^{-2}) and commercial Pd black (2.15 mA·cm^{-2}). Tafel plots of the three catalysts were determined from the ORR curves for further comparison of the ORR kinetics (Fig. 4(c)). Under 0.85V, Au@PdPb NWs display obviously higher kinetic current density ($j_{Au@PdPb\ NWs}$ = 2.48 mA·cm^{-2}) than the other two catalysts ($j_{Au@Pd\ NWs}$ = 1.38 mA·cm^{-2} and $j_{Pd\ black}$ = 0.61 mA·cm^{-2}), manifesting the best ORR kinetics on Au@PdPb NWs. The electron transfer numbers (n) of three electrocatalysts were calculated during the ORR process through the rotating ring-disk electrode (RRDE) curves (Fig. S7 in the ESM). As depicted in Fig. 4(d), the closer 4 transfer number and the lower H_2O_2 yield of Au@PdPb NWs signify a thoroughly one-step electro-reduction of oxygen into H_2O on Au@PdPb NWs [20]. Subsequently, the predominant ORR activity of Au@PdPb NWs was investigated via corresponding cyclic voltammetry (CV) curves (Fig. 4(e)). Electrochemical surface area (ECSA) of Au@PdPb NWs was calculated from the CV curve to be 12.82 m^2·g^{-1} with an error range of 5%, slightly higher than those of Au@Pd NWs (12.30 m^2·g^{-1}) and Pd black (11.9 m^2·g^{-1}) with error ranges of 8% and 6%, respectively. Meanwhile, the reduction peak potential of PdO in Au@PdPb NWs was about 57 and 70 mV more positive than those of Au@Pd NWs and Pd black, indicating faster desorption of hydroxyl species on the surface of Au@PdPb NWs, thus leading to the improved ORR activity [37, 38]. The ORR stability is also a key factor to evaluate catalysts. After the persistent chronoamperometry *i-t* test under 0.5 V for 10,000 s, the loss of the current density of Au@PdPb NWs was 42.7% (Fig. 4(f)), which was notably lower than 66.1% of Pd black and 47.91% of Au@Pd NWs, respectively. Then, ORR curves of the three electrocatalysts before and after the chronoamperometry were obtained for further comparison of the long-term durability. As shown in Fig. S8 in the ESM, the $E_{1/2}$ of Au@PdPb NWs is only negatively shifted by 16 mV, which is more stable than Au@Pd NWs ($\Delta E_{1/2}$ = 22 mV) and commercial Pd black ($\Delta E_{1/2}$ = 28 mV). TEM image and EDX spectrum of Au@PdPb NWs were conducted after the stability test. As shown in Fig. S9(a) in the ESM, the 1D nanowire struture of Au@PdPb NWs kept well without any structural collapse and aggregation during the ORR, which is ascribed to the good structural stability of the Au NWs core. There was almost no change of the relative content of Pd, but a little loss of Pb (0.8%) after the stability test (Fig. S9(b) in the ESM), implying an enhanced structural and component stability. In addition, CVs before and after continuous 100 cycles of CV scan were also performed as a direct electrocatalytic stability comparison (Fig. S10 in the ESM). By calculating the ECSA, the loss of Au@PdPb NWs is 8% after the 100 CV scan cycles, significantly superior to 13% of Au@Pd NWs and 20% of commercial Pd black, indicating the excellent long-term catalytic stability of Au@PdPb NWs in acid media.

Since ultrathin Au NWs almost have no ORR activity (Fig. S11 in the ESM) based on the intrinsic metal property of Au, PdPb may be the main active sites in Au@PdPb NWs. To deeply interpret the effect of Au and Pb on the electronic structure of Pd and the resulted predominant ORR performance of Au@PdPb NWs, the metal valence and electronic state of surface atoms of the nanowire samples were examined by X-ray photoelectron spectroscopy (XPS) [39, 40]. Figure 5(a) reveals the Au 4f XPS of Au NWs, Au@Pd NWs, and Au@PdPb NWs. The fitting peaks at the binding energy (BE) of around 84.0 and 88.0 eV can be assigned to zero valent state of Au. Figure 5(b) shows

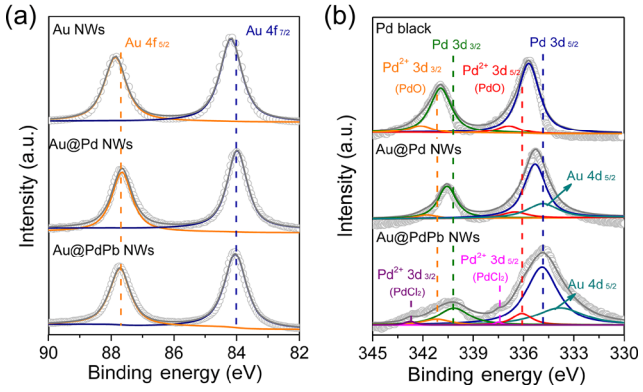

Figure 5 (a) High-resolution Au 4f XPS of Au NWs, Au@Pd NWs, and Au@PdPb NWs. (b) High-resolution Pd 3d XPS of Pd black, Au@Pd NWs, and Au@PdPb NWs.

the Pd 3d XPS of Au@Pd NWs and Au@PdPb NWs in contrast with Pd black. The contents of Pd^0 in Au@PdPb NWs, Au@Pd NWs, and Pd black were 88.1%, 88.3%, and 89.7%, respectively, confirming the effective reduction of Pd in the NWs [41]. However, the Pb^0 only occupied 14.3% among all the Pb elements (Fig. S12 in the ESM), which might be ascribed to the oxidation of Pb under the exposure in air and can prevent the oxidation of Pd to some extent [19]. It is worth noting that Au 4f core level of different catalysts reveals that the Au 4f binding energies of Au@PdPb NWs were negatively shifted compared to those of Au@Pd NWs and Au NWs (Fig. 5(a)). The Pd 3d core level of Au@PdPb NWs was also observed to shift to lower binding energy with respect to that for Pd black and Au@Pd NWs (Fig. 5(b)). The negative shift of Pd 3d binding energies in Au@PdPb NWs may be made by the difference in work function between Au and PdPb alloy, accompanied by rehybridization of the d-band [42]. Considering the high correlation between valence band XPS and metal d-band center [43, 44], the d-band center of Pd in Au@PdPb NWs should shift downward compared to that of Pd black and Au@Pd NWs. It was reported that the reaction rate catalyzed by the core–shell catalysts increases as the d-band center of shell metal is shifted more negatively with respect to Fermi level owing to the decreased adsorption strength of intermediates [45–48]. Therefore, the modification of electronic structure through a charge transfer between core and shell elements plays a key role in determining the ORR activity of Au@PdPb NWs, as it can optimize binding affinity for oxygen species on Au@PdPb NWs surface [49].

The excellent ORR activity and stability might be attributed to the following reasons: (1) Ultrathin Au NWs used in this work act as an important hard template, leading to Au@PdPb NWs with well-defined ultrathin and ultralong 1D nanostructures. In comparison with 0D commercial Pd black nanoparticles, 1D ultrathin Au@PdPb NWs can effectively prevent the dissolution, agglomeration, and Ostwald ripening of electrocatalysts during the ORR electrocatalysis, and hence exhibit a higher structural stability [14, 29, 31]. (2) Au NWs functioning as important support and substrate are more chemically stable and inactive under the ORR potential range in the acidic electrolyte (1.0 M $HClO_4$), which can efficaciously obstruct the activity loss arising from the support corrosion and structure collapse under high potentials [50, 51]. In addition, the Au atoms on the subsurface of Au@PdPb NWs can also lead to the enhanced stability of the surficial PdPb alloy layers via the place-exchange mechanism [51–53]. (3) Notably, the introduction of Au as the core can effectively modify the electronic structure of the PdPb alloy shell, thus decreasing adsorption strength of oxygen species on Au@PdPb NWs surface to enhance the ORR activity [47–49].

3 Conclusions

In summary, we demonstrated the successful synthesis of trimetallic core–shell Au@PdPb nanowires via using pre-fabricated Au nanowires as the template for boosting ORR in acidic media. The as-prepared Au@PdPb NWs were demonstrated to be active and stable for the ORR, much better than those of commercial Pd black and bimetallic Au@Pd NWs. The anisotropic 1D structure could favor the mass/electron transfer, increase the atomic utilization, and offer robust structural stability of Au@PdPb NWs, while the integration of Au and Pb was critical for optimizing electronic structure of Pd, which could downshift d-band center, and thus weaken the binding of oxygenated species to Pd and enhance the ORR activity. Considering the facile synthesis method and excellent ORR performance, the developed Au@PdPb NWs may have great potential in the field of fuel cells.

Acknowledgements

This work was supported by the Academic Research Fund (AcRF) Tier 1 Grant (No. RG105/19) from the Ministry of Education in Singapore, the National Natural Science Foundation of China (No. 21875112), and the China Scholarship Council (No. 201906090199).

Electronic Supplementary Material: Supplementary material (experimental sections, TEM, HRTEM and HAADF-STEM images, EDX spectra, XPS, supporting CV, LSV, and *i-t* curves) is available in the online version of this article at https://doi.org/10.1007/s12274-020-2911-9.

References

[1] Shen, H. J.; Gracia-Espino, E.; Ma, J. Y.; Zang, K. T.; Luo, J.; Wang, L.; Gao, S. S.; Mamat, X.; Hu, G. Z.; Wagberg, T. et al. Synergistic effects between atomically dispersed Fe-N-C and C-S-C for the oxygen reduction reaction in acidic media. *Angew. Chem., Int. Ed.* **2017**, *56*, 13800–13804.

[2] Shao, M. H.; Chang, Q. W.; Dodelet, J. P.; Chenitz, R. Recent advances in electrocatalysts for oxygen reduction reaction. *Chem. Rev.* **2016**, *116*, 3594–3657.

[3] Li, J. C.; Cheng, M.; Li, T.; Ma, L.; Ruan, X. F.; Liu, D.; Cheng, H. M.; Liu, C.; Du, D.; Wei, Z. D. et al. Carbon nanotube-linked hollow carbon nanospheres doped with iron and nitrogen as single-atom catalysts for the oxygen reduction reaction in acidic solutions. *J. Mater. Chem. A* **2019**, *7*, 14478–14482.

[4] Jiao, W. L.; Chen, C.; You, W. B.; Chen, G. Y.; Xue, S. Y.; Zhang, J.; Liu, J. W.; Feng, Y. Z.; Wang, P.; Wang, Y. Z. et al. Tuning strain effect and surface composition in PdAu hollow nanospheres as highly efficient ORR electrocatalysts and SERS substrates. *Appl. Catal. B Environ.* **2020**, *262*, 118298.

[5] Luo, M. C.; Zhao, Z. L.; Zhang, Y. L.; Sun, Y. J.; Xing, Y.; Lv, F.; Yang, Y.; Zhang, X.; Hwang, S.; Qin, Y. N. et al. PdMo bimetallene for oxygen reduction catalysis. *Nature* **2019**, *574*, 81–85.

[6] Bu, L. Z.; Shao, Q.; Pi, Y. C.; Yao, J. L.; Luo, M. C.; Lang, J. P.; Hwang, S.; Xin, H. L.; Huang, B. L.; Guo, J. et al. Coupled *s-p-d* exchange in facet-controlled Pd_3Pb tripods enhances oxygen reduction catalysis. *Chem* **2018**, *4*, 359–371.

[7] Chen, D.; Li, C. Y.; Liu, H.; Ye, F.; Yang, J. Core-shell Au@Pd nanoparticles with enhanced catalytic activity for oxygen reduction reaction via core-shell Au@Ag/Pd constructions. *Sci. Rep.* **2015**, *5*, 11949.

[8] Chen, D.; Sun, P. C.; Liu, H.; Yang, J. Bimetallic Cu–Pd alloy multipods and their highly electrocatalytic performance for formic acid oxidation and oxygen reduction. *J. Mater. Chem. A* **2017**, *5*,

4421–4429.
[9] Liu, R.; Zhang, L. Q.; Yu, C.; Sun, M. T.; Liu, J. F.; Jiang, G. B. Atomic-level-designed catalytically active palladium atoms on ultrathin gold nanowires. *Adv. Mater.* **2017**, *29*, 1604571.
[10] Hong, W.; Wang, J.; Wang, E. Dendritic Au/Pt and Au/PtCu nanowires with enhanced electrocatalytic activity for methanol electrooxidation. *Small* **2014**, *10*, 3262–3265.
[11] Yang, C. W.; Chanda, K.; Lin, P. H.; Wang, Y. N.; Liao, C. W.; Huang, M. H. Fabrication of Au-Pd core-shell heterostructures with systematic shape evolution using octahedral nanocrystal cores and their catalytic activity. *J. Am. Chem. Soc.* **2011**, *133*, 19993–20000.
[12] Bu, L. Z.; Tang, C. Y.; Shao, Q.; Zhu, X.; Huang, X. Q. Three-dimensional Pd_3Pb nanosheet assemblies: High-performance non-Pt electrocatalysts for bifunctional fuel cell reactions. *ACS Catal.* **2018**, *8*, 4569–4575.
[13] Fang, C.; Bi, T.; Ding, Q.; Cui, Z.; Yu, N.; Xu, X.; Geng, B. High-density Pd nanorod arrays on Au nanocrystals for high-performance ethanol electrooxidation. *ACS Appl. Mater. Interfaces* **2019**, *11*, 20117–20124.
[14] Xue, Q.; Bai, J.; Han, C. C.; Chen, P.; Jiang, J. X.; Chen, Y. Au nanowires@Pd-polyethylenimine nanohybrids as highly active and methanol-tolerant electrocatalysts toward oxygen reduction reaction in alkaline media. *ACS Catal.* **2018**, *8*, 11287–11295.
[15] Hernández, A. R.; Manríquez, M. E.; Mejia, A. E.; Estrada, E. M. A. Shape effect of AuPd core-shell nanostructures on the electrocatalytical activity for oxygen reduction reaction in acid medium. *Electrocatalysis* **2018**, *9*, 752–761.
[16] Zong, Z.; Xu, K. B.; Li, D. L.; Tang, Z. H.; He, W.; Liu, Z.; Wang, X. F.; Tian, Y. Peptide templated Au@Pd core-shell structures as efficient bi-functional electrocatalysts for both oxygen reduction and hydrogen evolution reactions. *J. Catal.* **2018**, *361*, 168–176.
[17] Yang, L.; Li, G. Q.; Chang, J. F.; Ge, J. J.; Liu, C. P.; Vladimir, F.; Wang, G. L.; Jin, Z.; Xing, W. Sea urchin-like $Au_{core}@Pd_{shell}$ electrocatalysts with high FAOR performance: Coefficient of lattice strain and electrochemical surface area. *Appl. Catal. B Environ.* **2020**, *260*, 118200.
[18] Chen, D.; Li, J. Q.; Cui, P. L.; Liu, H.; Yang, J. Gold-catalyzed formation of core-shell gold-palladium nanoparticles with palladium shells up to three atomic layers. *J. Mater. Chem. A* **2016**, *4*, 3813–3821.
[19] Wang, K.; Qin, Y. N.; Lv, F.; Li, M. Q.; Liu, Q.; Lin, F.; Feng, J. R.; Yang, C.; Gao, P.; Guo, S. J. Intermetallic Pd_3Pb nanoplates enhance oxygen reduction catalysis with excellent methanol tolerance. *Small Methods* **2018**, *2*, 1700331.
[20] Deng, Y. Y.; Xue, H. R.; Lu, S. L.; Song, Y. J.; Cao, X. Q.; Wang, L.; Wang, H. J.; Zhao, Y. L.; Gu, H. W. Trimetallic Au@PtPd mesoporous nanorods as efficient electrocatalysts for the oxygen reduction reaction. *ACS Appl. Energy Mater.* **2018**, *1*, 4891–4898.
[21] Tsuji, M.; Takemura, K.; Shiraishi, C.; Ikedo, K.; Uto, K.; Yajima, A.; Hattori, M.; Nakashima, Y.; Fukutomi, K.; Tsuruda, K. et al. Syntheses of Au@PdAg and Au@PdAg@Ag core-shell nanorods through distortion-induced alloying between Pd shells and Ag atoms over Au nanorods. *J. Phys. Chem. C* **2015**, *119*, 10811–10823.
[22] Shang, C. S.; Hong, W.; Wang, J.; Wang, E. Carbon supported trimetallic nickel-palladium-gold hollow nanoparticles with superior catalytic activity for methanol electrooxidation. *J. Power Sources* **2015**, *285*, 12–15.
[23] Luo, L. M.; Zhang, R. H.; Chen, D.; Hu, Q. Y.; Zhou, X. W. Synthesis of 3D thornbush-like trimetallic CoAuPd nanocatalysts and electrochemical dealloying for methanol oxidation and oxygen reduction reaction. *ACS Appl. Energy Mater.* **2018**, *1*, 2619–2629.
[24] Li, X. K.; Zhang, C. M.; Du, C.; Zhuang, Z. H.; Zheng, F. Q.; Li, P.; Zhang, Z. W.; Chen, W. Trimetallic Au@PdPt core-shell nanoparticles with ultrathin PdPt skin as highly stable electrocatalysts for the oxygen reduction reaction in acid solution. *Sci. China Chem.* **2019**, *62*, 378–384.
[25] He, D. S.; He, D. P.; Wang, J.; Lin, Y.; Yin, P. Q.; Hong, X.; Wu, Y.; Li, Y. D. Ultrathin icosahedral Pt-enriched nanocage with excellent oxygen reduction reaction activity. *J. Am. Chem. Soc.* **2016**, *138*, 1494–1497.
[26] Wang, L.; Yamauchi, Y. Metallic nanocages: Synthesis of bimetallic Pt-Pd hollow nanoparticles with dendritic shells by selective chemical etching. *J. Am. Chem. Soc.* **2013**, *135*, 16762–16765.
[27] Lv, H.; Sun, L. Z.; Xu, D. D.; Henzie, J.; Yamauchi, Y.; Liu, B. Mesoporous palladium-boron alloy nanospheres. *J. Mater. Chem. A* **2019**, *7*, 24877–24883.
[28] Yan, X. X.; Hu, X. J.; Fu, G. T.; Xu, L.; Lee, J. M.; Tang, Y. W. Facile synthesis of porous Pd_3Pt half-shells with rich "active sites" as efficient catalysts for formic acid oxidation. *Small* **2018**, *14*, 1703940.
[29] Gong, M. X.; Deng, Z. P.; Xiao, D. D.; Han, L. L.; Zhao, T. H.; Lu, Y.; Shen, T.; Liu, X. P.; Lin, R. Q.; Huang, T. et al. One-nanometer-thick Pt_3Ni bimetallic alloy nanowires advanced oxygen reduction reaction: Integrating multiple advantages into one catalyst. *ACS Catal.* **2019**, *9*, 4488–4494.
[30] Jiang, X.; Qiu, X. Y.; Fu, G. T.; Sun, J. Z.; Huang, Z. N.; Sun, D. M.; Xu, L.; Zhou, J. C.; Tang, Y. W. Highly simple and rapid synthesis of ultrathin gold nanowires with (111)-dominant facets and enhanced electrocatalytic properties. *J. Mater. Chem. A* **2018**, *6*, 17682–17687.
[31] Jiang, X.; Fu, G. T.; Wu, X.; Liu, Y.; Zhang, M. Y.; Sun, D. M.; Xu, L.; Tang, Y. W. Ultrathin AgPt alloy nanowires as a high-performance electrocatalyst for formic acid oxidation. *Nano Res.* **2018**, *11*, 499–510.
[32] Fu, G. T.; Jiang, X.; Chen, Y. F.; Xu, L.; Sun, D. M.; Lee, J. M.; Tang, Y. W. Robust bifunctional oxygen electrocatalyst with a "rigid and flexible" structure for air-cathodes. *NPG Asia Mater.* **2018**, *10*, 618–629.
[33] Li, M. F.; Zhao, Z. P.; Cheng, T.; Fortunelli, A.; Chen, C. Y.; Yu, R.; Zhang, Q. H.; Gu, L.; Merinov, B. V.; Lin, Z. Y. et al. Ultrafine jagged platinum nanowires enable ultrahigh mass activity for the oxygen reduction reaction. *Science* **2016**, *354*, 1414–1419.
[34] Feng, Y. G.; Bu, L. Z.; Guo, S. J.; Guo, J.; Huang, X. Q. 3D platinum-lead nanowire networks as highly efficient ethylene glycol oxidation electrocatalysts. *Small* **2016**, *12*, 4464–4470.
[35] Jiang, X.; Wang, J. X.; Huang, T.; Fu, G. T.; Tang, Y. W.; Qiu, X. Y.; Zhou, J. C.; Lee, J. M. Sub-5 nm palladium nanoparticles *in situ* embedded in N-doped carbon nanoframes: Facile synthesis, excellent sinter resistance and electrocatalytic properties. *J. Mater. Chem. A* **2019**, *7*, 26243–26249.
[36] Fu, G. T.; Liu, Y.; Wu, Z. X.; Lee, J. M. 3D robust carbon aerogels immobilized with Pd_3Pb nanoparticles for oxygen reduction catalysis. *ACS Appl. Nano Mater.* **2018**, *1*, 1904–1911.
[37] Fu, G. T.; Jiang, X.; Gong, M. X.; Chen, Y.; Tang, Y. W.; Lin, J.; Lu, T. H. Highly branched platinum nanolance assemblies by polyallylamine functionalization as superior active, stable, and alcohol-tolerant oxygen reduction electrocatalysts. *Nanoscale* **2014**, *6*, 8226–8234.
[38] Zhao, Y. P.; Tao, L.; Dang, W.; Wang, L. L.; Xia, M. R.; Wang, B.; Liu, M. M.; Gao, F. M.; Zhang, J. J.; Zhao, Y. F. High-indexed PtNi alloy skin spiraled on Pd nanowires for highly efficient oxygen reduction reaction catalysis. *Small* **2019**, *15*, 1900288.
[39] Li, T. F.; Wang, Y.; Tang, Y. Z.; Xu, L.; Si, L.; Fu, G. T.; Sun, D. M.; Tang, Y. W. White phosphorus derived PdAu-P ternary alloy for efficient methanol electrooxidation. *Catal. Sci. Technol.* **2017**, *7*, 3355–3360.
[40] Liu, Z. Y.; Fu, G. T.; Li, J. H.; Liu, Z. Q.; Xu, L.; Sun, D. M.; Tang, Y. W. Facile synthesis based on novel carbon-supported cyanogel of structurally ordered Pd_3Fe/C as electrocatalyst for formic acid oxidation. *Nano Res.* **2018**, *11*, 4686–4696.
[41] Yang, D. J.; Kamienchick, I.; Youn, D. Y.; Rothschild, A.; Kim, I. D. Ultrasensitive and highly selective gas sensors based on electrospun SnO_2 nanofibers modified by Pd loading. *Adv. Funct. Mater.* **2010**, *20*, 4258–4264.
[42] Weinert, M.; Watson, R. E. Core-level shifts in bulk alloys and surface adlayers. *Phys. Rev. B* **1995**, *51*, 17168–17180.
[43] Fu, G. T.; Liu, Z. Y.; Chen, Y.; Lin, J.; Tang, Y. W.; Lu, T. H. Synthesis and electrocatalytic activity of Au@Pd core-shell nanothorns for the oxygen reduction reaction. *Nano Res.* **2014**, *7*, 1205–1214.
[44] Wakisaka, M.; Mitsui, S.; Hirose, Y.; Kawashima, K.; Uchida, H.; Watanabe, M. Electronic structures of Pt-Co and Pt-Ru alloys for CO-tolerant anode catalysts in polymer electrolyte fuel cells studied by EC−XPS. *J. Phys. Chem. B* **2006**, *110*, 23489–23496.
[45] Luan, C. L.; Zhou, Q. X.; Wang, Y.; Xiao, Y.; Dai, X. P.; Huang, X. L.; Zhang, X. A general strategy assisted with dual reductants and dual protecting agents for preparing Pt-based alloys with high-index facets and excellent electrocatalytic performance. *Small* **2017**, *13*,

1702617.

[46] Geng, J. R.; Zhu, Z.; Bai, X. X.; Li, F. J.; Chen, J. Hot-injection synthesis of $PtCu_3$ concave nanocubes with high-index facets for electrocatalytic oxidation of methanol and formic acid. *ACS Appl. Energy Mater*. **2020**, *3*, 1010–1016.

[47] Zhang, P. F.; Dai, X. P.; Zhang, X.; Chen, Z. K.; Yang, Y.; Sun, H.; Wang, X. B.; Wang, H.; Wang, M. L.; Su, H. X. et al. One-pot synthesis of ternary Pt–Ni–Cu nanocrystals with high catalytic performance. *Chem. Mater*. **2015**, *27*, 6402–6410.

[48] Ganduglia-Pirovano, M. V.; Natoli, V.; Cohen, M. H.; Kudrnovský, J.; Turek, I. Potential, core-level, and *d* band shifts at transition-metal surfaces. *Phys. Rev. B* **1996**, *54*, 8892–8898.

[49] Lee, K.; Savadogo, O.; Ishihara, A.; Mitsushima, S.; Kamiya, N.; Ota, K. I. Methanol-tolerant oxygen reduction electrocatalysts based on Pd-3D transition metal alloys for direct methanol fuel Cells. *J. Electrochem. Soc*. **2006**, *153*, A20–A24.

[50] Tan, Y. M.; Fan, J. M.; Chen, G. X.; Zheng, N. F.; Xie, Q. J. Au/Pt and Au/Pt_3Ni nanowires as self-supported electrocatalysts with high activity and durability for oxygen reduction. *Chem. Commun*. **2011**, *47*, 11624–11626.

[51] Wang, C.; van der Vliet, D.; More, K. L.; Zaluzec, N. J.; Peng, S.; Sun, S. H.; Daimon, H.; Wang, G. F.; Greeley, J.; Pearson, J. et al. Multimetallic Au/$FePt_3$ nanoparticles as highly durable electrocatalyst. *Nano Lett*. **2011**, *11*, 919–926.

[52] You, H.; Zurawski, D. J.; Nagy, Z.; Yonco, R. M. *In-situ* X-ray reflectivity study of incipient oxidation of Pt(111) surface in electrolyte solutions. *J. Chem. Phys*. **1994**, *100*, 4699–4702.

[53] Komanicky, V.; Chang, K. C.; Menzel, A.; Markovic, N. M.; You, H.; Wang, X.; Myers, D. Stability and dissolution of platinum surfaces in perchloric acid. *J. Electrochem. Soc*. **2006**, *153*, B446–B451.